


A New Class of Cyclometalated Ruthenium Sensitizers of the Type $\hat{\text{C}}\hat{\text{N}}\hat{\text{N}}$ for Efficient Dye-Sensitized Solar Cells

Jeum-Jong Kim,[†] Hyunbong Choi,[†] Sanghyun Paek,[†] Chulwoo Kim,[†] Kimin Lim,[†] Myung-Jong Ju,[†] Hong Seok Kang,[‡] Moon-Sung Kang,[§] and Jaejung Ko^{*,†}

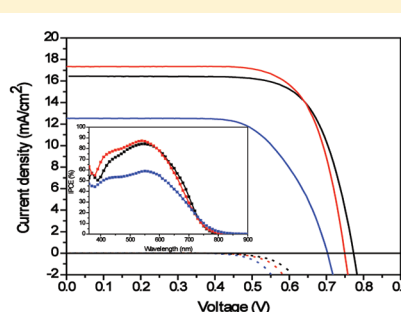
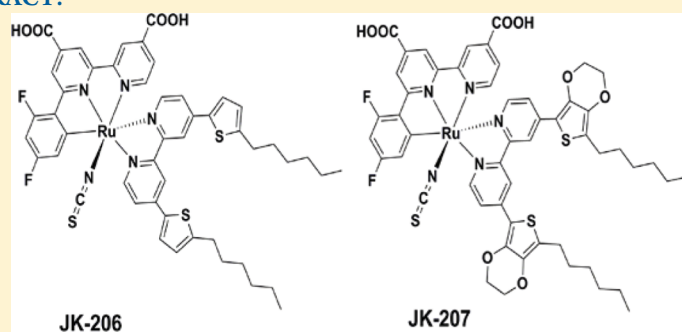
[†]Department of New Material Chemistry, Korea University, Jochiwon, Chungnam 339-700, Korea

[‡]Department of Nano and Advanced Materials, College of Engineering, Jeonju University, Jeonju, Korea

[§]Department of Environmental Engineering, College of Engineering, Sangmyung University, 300 Anseo-dong, Dongnam-gu, Cheonan, Chungnam Province 330-720, Republic of Korea

 Supporting Information

ABSTRACT:



A new class of cyclometalated ruthenium sensitizers incorporating a $\hat{\text{C}}\hat{\text{N}}\hat{\text{N}}$ ligand and conjugated 2,2'-bipyridine in the ancillary ligand have been designed and synthesized. The photovoltaic performance of **JK-206** using an electrolyte containing 0.6 M 1,2-dimethyl-3-propylimidazolium iodide, 0.05 M I_2 , 0.1 M LiI, and 0.5 M *tert*-butylpyridine in CH_3CN gave a short-circuit photocurrent density of 19.63 mA cm^{-2} , an open-circuit voltage of 0.74 V, and a fill factor of 0.72, affording an overall conversion efficiency of 10.39%. The efficiency is the highest one reported for dye-sensitized solar cells based on the cyclometalated ruthenium sensitizer of the type $\hat{\text{C}}\hat{\text{N}}\hat{\text{N}}$. Moreover, the same device using a polymer gel electrolyte exhibited a remarkable stability under 1000 h of light soaking at 60°C , retaining 91% of the initial efficiency of 7.14%.

INTRODUCTION

Dye-sensitized solar cells (DSSCs) based on mesoporous TiO_2 electrodes have attracted widespread attention because of their low-cost fabrication and high power conversion efficiency.¹ The photovoltaic performance of DSSCs has been rapidly improved by molecular engineering of the sensitizer,² minimization of the interfacial charge recombination,³ and the development of some additives.⁴ In these cells, the sensitizer is one of the key components in achieving a high conversion efficiency. Several poly(pyridylruthenium) complexes⁵ have achieved power conversion efficiencies of over 11% in standard air mass 1.5 sunlight. In spite of their high photovoltaic performances, the efficiency of DSSCs still needs to be improved in order to become competitive with conventional photovoltaic cells. The design of an optimal sensitizer with a red-shifted absorption band and increasing molar absorption coefficient presents a challenging task. Our strategy is to find ways to systematically shift the metal-to-ligand charge-transfer (MLCT) band toward the red region of the dye. In the first approach, the judicious tuning of the highest occupied molecular orbital (HOMO) and lowest unoccupied molecular

orbital (LUMO) levels of a dye by changing the substituent is an attractive route to the panchromatic sensitization of TiO_2 electrodes.⁶ The second approach for broadening the absorption band and increasing the molar absorption coefficient is to increase the conjugation length of the bipyridyl ligand.⁷ Such an increase can be achieved by replacing one of the 4,4'-dicarboxy-2,2'-bipyridine (dcbpy) anchoring ligands in N3 with a highly conjugated ancillary group such as thiophene⁸ and alkoxybenzene moieties.⁹ In the third approach, the replacement of a neutral $\text{Ru}-\text{N}$ bond with an anionic $\text{Ru}-\text{C}$ bond in a multidentate ligand is an effective strategy for shifting the MLCT band to the red region.¹⁰ The broad and red-shifted absorption properties of the cyclometalated complexes of ruthenium(II) render these as a new class of promising sensitizers because they are shown to dramatically change the electronic properties by raising the energy of their HOMO. Recently, Nazeeruddin et al.,¹¹ Ghadarr et al.,¹² van Koten et al.,¹² and Chi et al.¹³ reported thiocyanate-free

Received: April 26, 2011

Published: October 17, 2011

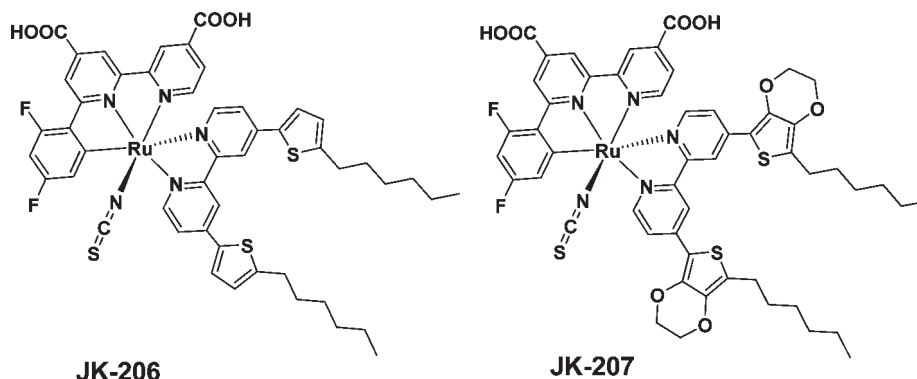


Figure 1. Molecular structures of JK-206 and JK-207.

cyclometalated ruthenium sensitizers of the type $\hat{\text{C}}\text{N}$, $\hat{\text{C}}\text{NN}$, $\hat{\text{N}}\text{N}$, and $\hat{\text{N}}\text{NN}$, which exhibit high power conversion efficiencies. Herein, we report a new type of cyclometalated ruthenium complex as efficient sensitizers, coded as JK-206 and JK-207, of the type $\hat{\text{C}}\text{NN}$, $\hat{\text{N}}\text{N}$, and NCS ligands. These novel ruthenium complexes exhibit remarkable performances as sensitizers. The thiophene-derived ancillary units were introduced for increasing the conjugation length to increase the light-harvesting ability and red-shift the MLCT band of ruthenium sensitizers. The role of one thiocyanato ligand is to easily regenerate the dye from the redox system.¹⁴ The molecular structures of the two ruthenium sensitizers are shown in Figure 1.

EXPERIMENTAL SECTION

General Methods. All reactions were carried out under an argon atmosphere. Solvents were distilled from the appropriate reagents. All reagents were purchased from Sigma-Aldrich. Dimethyl 2,2'-bipyridine-4,4'-dicarboxylate (1),¹⁵ 4,4'-bis(5-hexylthiophen-2-yl)-2,2'-bipyridine,¹⁶ and 4,4'-bis(7-hexylethylenedioxythiophen-2-yl)-2,2'-bipyridine¹⁷ were synthesized using a modified procedure of previous references. ¹H and ¹³C NMR spectra were recorded on a Varian Mercury 300 spectrometer. Elemental analyses were performed with a Carlo Erba Instruments CHNS-O EA 1108 analyzer. Mass spectra were recorded on a JEOL JMS-SX102A instrument. The absorption and photoluminescence spectra were recorded on a Perkin-Elmer Lambda 2S UV-vis spectrometer and a Perkin-Elmer LS fluorescence spectrometer, respectively.

Fabrication of DSSC. FTO glass plates (Pilkington TEC Glass-TEC 8, Solar 2.3 mm thickness) were cleaned in a detergent solution using an ultrasonic bath for 30 min and rinsed with water and ethanol. The FTO glass plates were immersed in 40 mM TiCl₄(aq) at 70 °C for 30 min and washed with water and ethanol. A transparent nanocrystalline layer on the FTO glass plate was prepared by doctor blade printing TiO₂ paste (Solaronix, Ti-Nanoxide D20, 20 nm) and then dried for 2 h at 25 °C. The TiO₂ electrodes were gradually heated under an air flow at 325 °C for 5 min, at 375 °C for 5 min, at 450 °C for 15 min, and at 500 °C for 15 min. The thickness of the transparent layer was measured by using an Alpha-step 250 surface profilometer (Tencor Instruments, San Jose, CA). A paste for the scattering layer containing 400-nm-sized anatase particles (CCIC, PST-400C) was deposited by doctor blade printing and then dried for 2 h at 25 °C. The TiO₂ electrodes were gradually heated under an air flow at 325 °C for 5 min, at 375 °C for 5 min, at 450 °C for 15 min, and at 500 °C for 15 min. The resulting film was composed of a 10-μm-thick transparent layer and a 4-μm-thick scattering layer. The TiO₂ electrodes were treated again by TiCl₄ at 70 °C for 30 min and sintered at 500 °C for 30 min. The TiO₂ electrodes were immersed in JK-206, JK-207, and N719 [0.3 mM in EtOH containing

10 mM 3a,7a-dihydroxy-5b-cholic acid (Cheno)] and kept at room temperature overnight. The FTO plate for counter electrodes was cleaned with an ultrasonic bath in H₂O, acetone, and 0.1 M HCl(aq), subsequently. Counter electrodes were prepared by coating with a drop of H₂PtCl₆ solution (2 mg of platinum in 1 mL of ethanol) on an FTO plate and heating at 400 °C for 15 min. The dye-adsorbed TiO₂ electrode and platinum counter electrode were assembled into a sealed sandwich-type cell by heating at 80 °C with a hot-melt ionomer film (Surlyn) as a spacer between the electrodes. A drop of an electrolyte solution was placed on the drilled hole in the counter electrode of the assembled cell and was driven into the cell via vacuum backfilling. Two electrolytes were used for device evaluation. Electrolyte A: 0.6 M 1,2-dimethyl-3-propylimidazolium iodide (DMPH), 0.05 M iodine, 0.1 M LiI, and 0.5 M *tert*-butylpyridine (TBP) in acetonitrile. Electrolyte B: 0.1 M iodine, 0.5 M NMBI, and 5 wt % poly(vinylidene fluoride-co-hexafluoropropylene) (PVDF-HFP) in 3-methoxypropionitrile (MPN). Finally, the hole was sealed using additional Surlyn and a cover glass (0.1 mm thickness). The adsorbed quantity on TiO₂ films is calculated by the difference in the absorbance between 8-μm-thick TiO₂ films each coated with 5×10^{-4} M JK-206, JK-207, and N719 in *N,N*-dimethylformamide (DMF) and desorbed JK-206, JK-207, and N719 from their corresponding TiO₂ films into aqueous 10⁻² M KOH (2 mL) for 5 h.

Time-Dependent Density Functional Theory (TD-DFT) Calculations. Structure optimization was done with B3LYP/Lanl2dz. On the one hand, TD-DFT calculations were done using B3LYP with a mixed basis set, i.e., SDD ECP and 6-31+G(d,p) basis sets for Ru and other atoms, respectively.¹⁸ All of the calculations were done using the Gaussian03 program.¹⁹

Cyclic Voltamogram. Cyclic voltammetry was carried out with a BAS 100B (Bioanalytical Systems, Inc.) in combination with a conventional three-electrode, one-compartment electrochemical cell. A platinum foil and Ag/AgCl/KCl_{sat} were used as the counter and reference electrodes, respectively. A dye-coated nanocrystalline TiO₂ electrode was employed as the working electrode. The redox potential of dyes on TiO₂ was measured in CH₃CN with 0.1 M (*n*-C₄H₉)₄NPF₆ at a scan rate of 100 mV s⁻¹ [vs ferrocenium/ferrocene (Fc/Fc⁺)].

Characterization of Solar Cell Devices. *J*-*V* measurements were characterized under simulated 100 mW cm⁻² AM 1.5G irradiation from a 1000 W xenon arc lamp (Oriol 91193). The light intensity was adjusted with a silicon solar cell that was calibrated with an NREL-calibrated silicon solar cell (PV Measurement Inc.). The applied potential and measured cell current were measured using a Keithley model 2400 digital source meter. The incident photon-to-current conversion efficiency (IPCE) spectra for the cells were measured on an IPCE measuring system (PV Measurements Inc.). The light and thermal tests were performed with Suntest CPS/CPS+ equipment (AB Nexco Co).

Electron Transport Measurements. The electron diffusion coefficients (*D_e*) and lifetimes (*τ_e*) in the TiO₂ photoelectrode were

measured by the stepped light-induced transient measurements of the photocurrent and voltage.²⁰ The transients were induced by a stepwise change in the laser intensity. A diode laser ($\lambda = 635$ nm) as a light source was modulated using a function generator. The initial laser intensity was a constant 90 mW cm^{-2} and was attenuated up to approximately 10 mW cm^{-2} using a neutral density (ND) filter, which was positioned at the front side of the fabricated samples (TiO_2 film thickness = ca. $10 \mu\text{m}$; active area = 0.04 cm^2). The photocurrent and photovoltage transients were monitored using a digital oscilloscope through an amplifier. The D_e value was obtained by a time constant (τ_c) determined by fitting a decay of the photocurrent transient with $\exp(-t/\tau_c)$ and the TiO_2 film thickness (ω) using the equation $D_e = \omega^2/(2.77\tau_c)$.^{20a} The τ_c value was also determined by fitting a decay of the photovoltage transient with $\exp(-t/\tau_c)$.^{20a} All experiments were conducted at room temperature.

4,4'-Bis(methoxycarbonyl)-2,2'-bipyridine-1-oxide (2). To a CHCl_3 solution of 4,4'-bis(methoxycarbonyl)-2,2'-bipyridine (1.0 g, 3.67 mmol) was added slowly at room temperature 3-chloroperoxybenzoic acid (MCPBA; 821 mg, 3.67 mmol) as a solid. The reaction was continued for 10 h. The reaction solvent was removed under reduced pressure. The pure product 2 was obtained by column chromatography on silica gel (CH_2Cl_2 :MeOH = 30:1, $R_f = 0.42$). Yield: 78%. ^1H NMR (CDCl_3): δ 9.30 (dd, 1H, $J = 1.4$ Hz), 8.87 (dd, 1H, $J = 4.9$ Hz), 8.75 (d, 1H, $J = 2.4$ Hz), 8.32 (d, 1H, $J = 6.7$ Hz), 7.91 (dd, 1H, $J = 4.9$ Hz), 7.85 (d, 1H, $J = 6.8$ Hz), 3.95 (s, 3H), 3.93 (s, 3H). ^{13}C NMR (CDCl_3): δ 165.2, 163.9, 150.2, 149.9, 146.6, 141.0, 137.8, 128.3, 126.4, 125.3, 124.3, 123.8, 52.8, 52.7. Anal. Calcd for $\text{C}_{14}\text{H}_{12}\text{N}_2\text{O}_5$: C, 58.33; H, 4.20. Found: C, 58.12; H, 4.14.

Dimethyl-6-chloro-2,2'-bipyridine-4,4'-dicarboxylate (3). A mixture of 4,4'-bis(methoxycarbonyl)-2,2'-bipyridine-1-oxide (200 mg, 0.69 mmol) in POCl_3 (0.4 mL) was refluxed for 1.5 h. H_2O (50 mL) and CH_2Cl_2 (50 mL) were added. The organic layer was separated and dried with MgSO_4 . The solvent was removed under reduced pressure. The pure product 3 was obtained by column chromatography on silica gel using CH_2Cl_2 as the eluent ($R_f = 0.54$). Yield: 80%. ^1H NMR (CDCl_3): δ 8.87 (m, 3H), 7.91 (m, 2H), 4.00 (s, 3H), 3.99 (s, 3H). ^{13}C NMR (CDCl_3): δ 165.5, 164.4, 157.0, 155.1, 151.9, 150.2, 141.3, 138.8, 124.2, 123.8, 120.8, 119.2, 53.1, 52.9. Anal. Calcd for $\text{C}_{14}\text{H}_{11}\text{ClN}_2\text{O}_4$: C, 54.83; H, 3.62. Found: C, 54.51; H, 3.50.

Dimethyl-6-(2,4-difluorophenyl)-2,2'-bipyridine-4,4'-dicarboxylate (4). A mixture of 3 (260 mg, 0.85 mmol), 2,4-difluorophenylboronic acid pinacol ester (223 mg, 0.93 mmol), $\text{Pd}(\text{PPh}_3)_4$ (54 mg), and Na_2CO_3 (99 mg) was dissolved in tetrahydrofuran (THF; 50 mL)/ H_2O (10 mL), and the mixture was refluxed for 12 h. After evaporation of the solvent under reduced pressure, H_2O (50 mL) and CH_2Cl_2 (50 mL) were added. The organic layer was separated and dried with MgSO_4 . The solvent was removed under reduced pressure. The pure product 4 was obtained by column chromatography on silica gel using CH_2Cl_2 as the eluent ($R_f = 0.63$). Yield: 68%. ^1H NMR (CDCl_3): δ 8.98 (s, 1H), 8.89 (d, 1H, $J = 1.8$ Hz), 8.85 (d, 1H, $J = 5.1$ Hz), 8.34 (d, 1H, $J = 1.5$ Hz), 8.12 (s, 1H), 7.88 (dd, 1H, $J = 1.8$ and 1.5 Hz), 7.06 (m, 1H), 6.96 (m, 1H), 4.92 (s, 3H), 4.90 (s, 3H). ^{13}C NMR (CDCl_3): δ 165.7, 165.6, 156.4, 156.2, 152.9, 150.1, 139.3, 138.5, 132.3, 123.7, 123.6, 123.2, 120.5, 119.2, 112.2, 104.9, 104.5, 104.2, 52.8, 51.7. Anal. Calcd for $\text{C}_{20}\text{H}_{14}\text{F}_2\text{N}_2\text{O}_4$: C, 62.50; H, 3.67. Found: C, 62.38; H, 3.54.

6-(2,4-Difluorophenyl)-2,2'-bipyridine-4,4'-dicarboxylic Acid (5). A mixture of 4 (1.88 g, 4.89 mmol) and KOH (1.1 g, 4 eq) was dissolved in MeOH (50 mL)/ H_2O (10 mL), and the mixture was refluxed for 12 h. The reaction mixture was neutralized with a 2 M HCl solution, and the precipitate was filtered and washed with water and gave 1.6 g as a white solid. Yield: 92%. ^1H NMR ($\text{DMSO}-d_6$): δ 8.88 (d, 1H, $J = 5.7$ Hz), 8.79 (s, 1H), 8.75 (d, 1H, $J = 1.5$ Hz), 8.18 (s, 1H), 8.13 (s, 1H), 7.89 (d, 1H, $J = 1.5$ Hz), 7.43 (d, 1H, $J = 5.7$ Hz), 7.31 (m, 1H). ^{13}C NMR ($\text{DMSO}-d_6$): δ 166.4, 166.2, 156.0, 155.6, 152.6, 150.9, 140.9, 140.0, 132.7, 124.0, 123.5, 119.9, 119.1, 113.0, 112.7, 105.6, 105.3, 104.9.

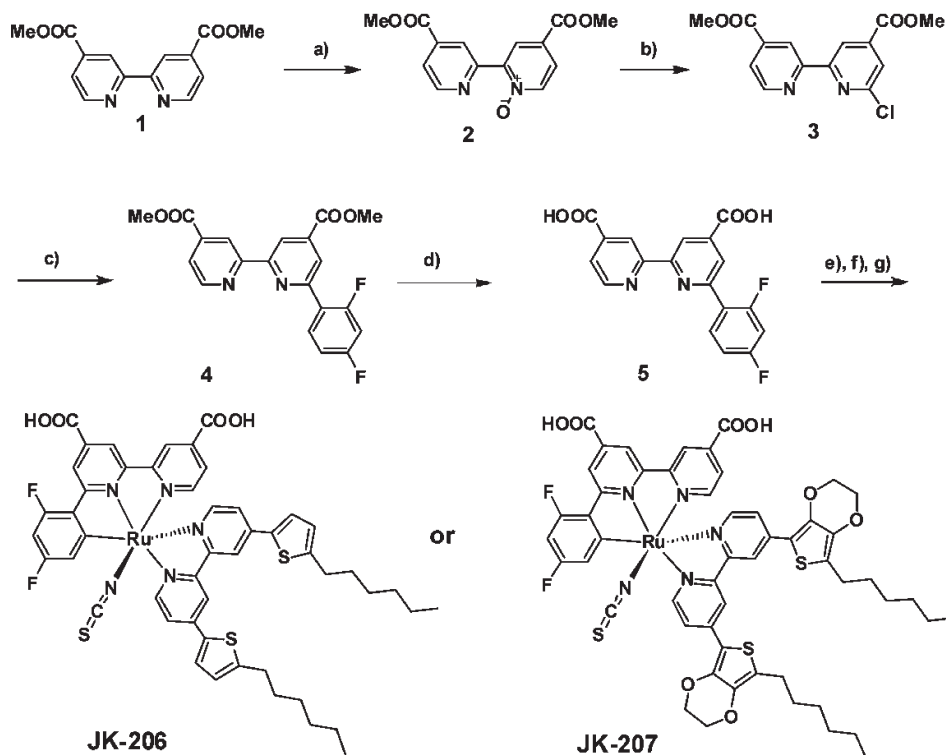
Anal. Calcd for $\text{C}_{18}\text{H}_{10}\text{F}_2\text{N}_2\text{O}_4$: C, 60.68; H, 2.83. Found: C, 60.41; H, 2.90.

Complex JK-206. A mixture 4,4'-bis(5-hexylthiophen-2-yl)-2,2'-bipyridine¹⁶ (137 mg, 0.28 mmol) and a dichloro(*p*-cymene)ruthenium(II) dimer (87 mg, 0.14 mmol) in argon-degassed DMF (15 mL) was stirred at 80°C for 4 h under reduced light. Subsequently, 6-(2,4-difluorophenyl)-2,2'-bipyridine-4,4'-dicarboxylic acid (100 mg, 0.28 mmol) was added into the flask, and the reaction mixture was stirred at 160°C for 4 h. An excess of NH_4NCS (126 mg, 1.42 mmol) was added to the resulting dark solution, and the reaction continued for another 8 h at 140°C . Then the reaction mixture was cooled to room temperature, and the solvent was removed under vacuum. Water was added to induce precipitation. The resulting solid was filtered, washed with water, and dried under vacuum. The resulting solid was dissolved in methanol containing 2.2 equiv of tetrabutylammonium hydroxide to confer solubility by deprotonating the carboxylic group and purified on a Sephadex LH-20 column with methanol as the eluent. The collected main band was concentrated, and the solution pH was lowered to 5.1 using 0.02 M nitric acid. The precipitate was collected on a sintered glass crucible by suction filtration and dried in air. Yield: 60%. MS (FAB, ^{101}Ru). Calcd for $\text{C}_{49}\text{H}_{45}\text{F}_2\text{N}_5\text{O}_4\text{RuS}_3$: m/z 1003.21. Found: m/z 1002.64 (M^+). ^1H NMR (CD_3OD): δ 9.59 (d, 1H, $J = 6.0$ Hz), 9.12 (s, 1H), 8.90 (s, 1H), 8.32 (d, 1H, $J = 3.3$ Hz), 8.29 (d, 1H, $J = 3.3$ Hz), 8.12 (s, 1H), 8.07 (s, 1H), 7.84 (m, 1H), 7.73 (s, 1H), 7.43 (s, 1H), 7.34 (m, 1H), 6.96 (m, 3H), 6.87 (m, 2H), 6.22 (m, 1H), 2.97 (t, 2H, $J = 4.2$ Hz), 2.90 (t, 2H, $J = 4.2$ Hz), 1.66 (m, 4H), 1.40 (m, 12H), 1.01 (m, 6H). Anal. Calcd for $\text{C}_{49}\text{H}_{45}\text{F}_2\text{N}_5\text{O}_4\text{RuS}_3$: C, 58.67; H, 4.52; N, 6.98. Found: C, 58.31; H, 4.42; N, 6.71.

Complex JK-207. A mixture 4,4'-bis(7-hexylethylenedioxythiophen-2-yl)-2,2'-bipyridine¹⁵ (270 mg, 0.44 mmol) and a dichloro(*p*-cymene)ruthenium(II) dimer (141 mg, 0.22 mmol) in argon-degassed DMF (15 mL) was stirred at 80°C for 4 h under reduced light. Subsequently, 6-(2,4-difluorophenyl)-2,2'-bipyridine-4,4'-dicarboxylic acid (159 mg, 0.44 mmol) was added into the flask, and the reaction mixture was stirred at 160°C for 4 h. An excess of NH_4NCS (195 mg, 2.20 mmol) was added to the resulting dark solution and the reaction continued for another 8 h at 140°C . Then, the reaction mixture was cooled to room temperature, and the solvent was removed under vacuum. Water was added to induce precipitation. The resulting solid was filtered, washed with water, and dried under vacuum. The resulting solid was dissolved in methanol containing 2.2 equiv of tetrabutylammonium hydroxide to confer solubility by deprotonating the carboxylic group and purified on a Sephadex LH-20 column with methanol as the eluent. The collected main band was concentrated, and the solution pH was lowered to 5.1 using 0.02 M nitric acid. The precipitate was collected on a sintered glass crucible by suction filtration and dried in air. Yield: 45%. MS (FAB, ^{101}Ru). Calcd for $\text{C}_{53}\text{H}_{49}\text{F}_2\text{N}_5\text{O}_8\text{RuS}_3$: m/z 1119.28. Found: m/z 1118.67 (M^+). ^1H NMR (CD_3OD): δ 9.47 (d, 1H, $J = 3.3$ Hz), 9.08 (s, 1H), 8.90 (d, 1H, $J = 1.2$ Hz), 8.37 (m, 3H), 8.14 (d, 1H, $J = 4.2$ Hz), 7.48 (s, 1H), 7.37 (m, 1H), 7.23 (d, 1H, $J = 2.7$ Hz), 7.14 (d, 1H, $J = 3.6$ Hz), 7.04 (m, 1H), 6.36 (m, 1H), 4.50–4.25 (m, 8H), 2.76 (t, 2H, $J = 4.5$ Hz), 2.66 (t, 2H, $J = 4.2$ Hz), 1.63 (m, 4H), 1.31 (m, 12H), 0.89 (m, 6H). Anal. Calcd for $\text{C}_{53}\text{H}_{49}\text{F}_2\text{N}_5\text{O}_8\text{RuS}_3$: C, 56.87; H, 4.41; N, 6.26. Found: C, 56.61; H, 4.35; N, 6.08.

RESULTS AND DISCUSSION

The two cyclometalated ruthenium sensitizers JK-206 and JK-207 were synthesized by the stepwise synthetic protocol illustrated in Scheme 1. The dimethyl-6-chloro-2,2'-bipyridine-4,4'-dicarboxylate 3 was prepared by the oxidation reaction of 4,4'-bis(methoxycarbonyl)-2,2'-bipyridine with MCPBA, followed by chlorination of 2 with POCl_3 . The Suzuki coupling reaction²¹ of 3 with 2,4-difluorophenylboronic acid yielded 4. The hydrolysis

Scheme 1. Schematic Diagram for the Synthesis of Ruthenium Sensitizers JK-206 and JK-207^a

^a Reagents: (a) MCPBA, CH₂Cl₂; (b) POCl₃; (c) 2,4-difluorophenylboronic acid pinacol ester, Pd(PPh₃)₄, Na₂CO₃, THF, 80 °C; (d) KOH, aqueous MeOH; (e) for **JK-206**, 4,4'-bis(5-hexylthiophen-2-yl)-2,2'-bipyridine; for **JK-207**, 4,4'-bis(7-hexylethylenedioxythiophen-2-yl)-2,2'-bipyridine, [Ru(Cl)₂(*p*-cymene)]₂, DMF, 80 °C; (f) 6-(2,4-difluorophenyl)-2,2'-bipyridine-4,4'-dicarboxylic acid, DMF, 160 °C; (g) NH₄NCS, DMF, 140 °C.

reaction of **4** with aqueous KOH was converted to the $\hat{N}\hat{N}\hat{C}$ ligand **5**. **JK-206** and **JK-207** were synthesized in a one-pot reaction from the sequential reaction of [Ru(*p*-cymene)Cl₂]₂ with 4,4'-bis(5-hexylthiophen-2-yl)-2,2'-bipyridine or 4,4'-bis(7-hexylethylenedioxythiophen-2-yl)-2,2'-bipyridine, followed by the reaction of the resulting ruthenium intermediates with **5**. The chlororuthenium complexes reacted with an excess of ammonium thiocyanate to give the ruthenium sensitizers **JK-206** and **JK-207**.

Figure 2 shows the UV/vis spectra of **JK-206** and **JK-207** in EtOH as well as that of **N719** for reference and also shows normalized emission spectra. The absorption spectrum of **JK-206** exhibits two peaks at 391 and 527 nm, which are attributable to the MLCT transitions. The molar extinction coefficients of these two peaks are 19.8×10^3 and 18.0×10^3 M⁻¹ cm⁻¹, respectively (Table 1). The molar extinctions of the lower energy absorption bands of **JK-206** and **JK-207** increase 31% and 21% relative to that of **N719**. The low-energy MLCT band of **JK-207** is red-shifted about 3 and 10 nm compared with those of **JK-206** and **N719**. The red-shifted absorption is attributable to the electron-rich π -conjugation unit in an ancillary ligand. The cyclometalated complexes resulted in a broadening and red-shifted for the absorption band.^{10a} Such broadening and red shifting are desirable for harvesting the solar spectrum and lead to a large photocurrent.

The absorption spectra of **JK-206** on the TiO₂ film are significantly red-shifted and much broadened because of the *J* aggregation and interaction of the anchoring group with the surface titanium ions, ensuring a good light-harvesting efficiency. Excitation of the low-energy MLCT bands of **JK-206** and **JK-207** resulted in strong emissions centered at 800 and 795 nm, respectively.

We performed the molecular orbital calculation of **JK-206** and **JK-207** to gain insight into the photophysical properties using DFT and TD-DFT. Figure 3 presents the isodensity plots of frontier molecular orbitals of **JK-206** and **JK-207**.

The calculation illustrates that the band of the UV spectrum at 527 nm in **JK-206** is mainly characterized by a mixture of HOMO \rightarrow LUMO+2 (47%) and HOMO-1 \rightarrow LUMO+2 (19%). The HOMO is mainly populated over ruthenium t_{2g} character and thiocyanate with a significant contribution on the far-end S atom, while HOMO-1 is delocalized over the ruthenium center, -NCS, $\hat{N}\hat{N}\hat{C}$ unit, and bipyridyl ligand. The LUMO of **JK-206** is predominantly delocalized over the dcby portion of the $\hat{C}\hat{N}\hat{N}$ ligand, -NCS, and the ruthenium center. On the other hand, the LUMO+1 is delocalized over the bpy of the ancillary ligand. Examination of the HOMO and LUMO of both sensitizers indicates that HOMO-LUMO excitation moves the electron distribution from the Ru-NCS unit to the dcby moiety. Accordingly, the photoinduced electron transfer from the dye to the TiO₂ electrode can occur efficiently at the HOMO \rightarrow LUMO excitation.

The electrochemical properties of the two ruthenium sensitizers **JK-206** and **JK-207** were evaluated by cyclic voltammetry in CH₃CN with 0.1 M TBAPF₆. TiO₂ films stained with the sensitizers were used as working electrodes. Ferrocene was added to the solution, and the Fc/Fc⁺ redox couple was used as an internal potential reference. The potentials vs NHE were calculated by the addition of 630 mV to the potential vs Fc/Fc⁺. The oxidation potentials of the **JK-206** and **JK-207** sensitizers adsorbed on TiO₂ films show a quasi-reversible couple at 0.99 and 0.96 V vs NHE,

which is assigned to the $\text{Ru}^{\text{II/III}}$ couple, whereas the experimentally determined oxidation potential of **N719** using the same experimental conditions gave 1.13 V vs NHE. The 0.14–0.17 V cathodic shift of the **JK-206** and **JK-207** oxidation potentials relative to that of **N719** is attributed to the influence of the electron-donor nature of the ancillary ligand in both sensitizers. The oxidation potentials of both sensitizers are favorable for iodide oxidation.²² The excited-state reduction potentials of **JK-206** and **JK-207** calculated from the oxidation potential and E_{0-0} are summarized in Table 1. The excited-state oxidation potentials (E_{ox}^*) of the sensitizers (**JK-206**, –1.00 V; **JK-207**, –0.91 V vs NHE) were much more negative with respect to the conduction band edge of TiO_2 , providing the thermodynamic driving force for electron injection.²³

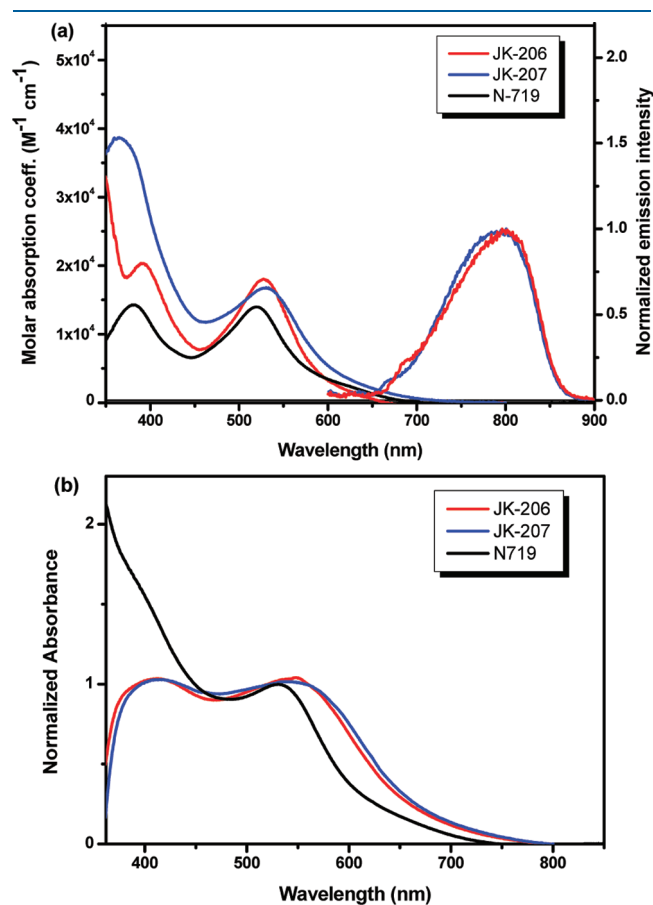


Figure 2. Absorption and emission spectra (a) of **JK-206** (red solid line), **JK-207** (blue solid line), and **N719** (black solid line) in EtOH and absorption spectra (b) of **JK-206** (red solid line), **JK-207** (blue solid line), and **N719** (black solid line) adsorbed on the TiO_2 film.

The inset of Figure 4 shows the photocurrent action spectrum of the **JK-206**, **JK-207**, and **N719** sensitized cells using an acetonitrile-based electrolyte. The cell was fabricated using a double layer of 9- μm -thick TiO_2 (20 nm) and 4- μm -thick scattering TiO_2 (400 nm). The band on the IPCE spectrum of **JK-206** tails off toward 830 nm and shows a performance of over 80% from 460 to 650 nm, peaking at 88% at 545 nm.

For reference, **N719** dye affords a maximum of 84% at 610 nm under the same conditions. The IPCE spectrum of **JK-206** is more enhanced in the 400–600 nm range compared to that of **N719** as a result of cyclometalation and extended π conjugation, which is consistent with the absorption spectrum of **JK-206**. From the overlap integral of the IPCE of **JK-206** with the standard global AM 1.5 solar emission spectrum, a short-circuit photocurrent density of 19.08 mA cm^{-2} is calculated, which is in good agreement with the measured photocurrent. The J – V curve for the devices based on **JK-206** and **JK-207** is shown and compared with that of **N719** in Figure 4. Under standard global AM 1.5 solar conditions, the **JK-206** and **JK-207** sensitized cells gave short-circuit photocurrent densities (J_{sc}) of 19.63 and 13.86 mA cm^{-2} , open-circuit voltages (V_{oc}) of 0.74 and 0.69 V, and fill factors (ff) of 0.72 and 0.66, corresponding to overall conversion efficiencies (η) of 10.39% and 6.32%, respectively (Table 1). Under the same conditions, the **N719** sensitized cell gave a J_{sc} of 18.79 mA cm^{-2} , a V_{oc} of 0.75 V, and a ff of 0.70, corresponding to η of 9.80%. The significant decrease in the η value for **JK-207** compared to a **JK-206**-based device demonstrates some role of the electron-donor ethylenedioxythiophen-2-yl

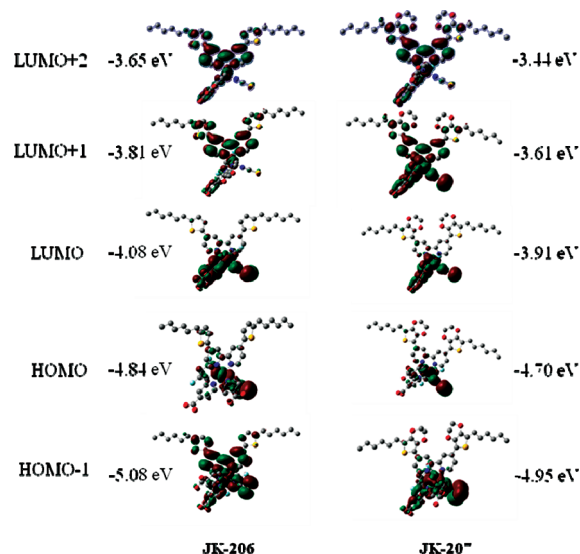


Figure 3. Isodensity surface plots of the HOMO, HOMO–1, LUMO, LUMO+1, and LUMO+2 of **JK-206** and **JK-207**.

Table 1. Optical, Redox, and DSSC Performance Parameters of Dyes

dye	λ_{abs}^a (nm) ($\epsilon/\text{M}^{-1} \text{ cm}^{-1}$)	E_{redox}^b (V)	E_{0-0}^c (V)	E_{LUMO}^d (V)	J_{sc} (mA cm^{-2})	V_{oc} (V)	FF	η^e (%)
JK-206	391 (19 800), 527 (18 000)	0.99	1.99	–1.00	19.63	0.74	0.72	10.39
JK-207	368 (38 700), 530 (16 800)	0.96	1.87	–0.91	13.86	0.69	0.66	6.32
N719	380 (13 100), 520 (1300)	1.13	2.29	–1.16	18.79	0.75	0.70	9.80

^a Absorption spectra were measured in an EtOH solution. ^b Redox potentials of dyes on TiO_2 were measured in CH_3CN with 0.1 M $(n\text{-C}_4\text{H}_9)_4\text{NPF}_6$ at a scan rate of 100 mV s^{-1} (vs NHE). ^c E_{0-0} values were estimated from the onset of the absorption spectrum. ^d E_{LUMO} was calculated by $E_{\text{ox}} - E_{0-0}$. ^e Performances of DSSCs were measured with a 0.18 cm^2 working area. The aperture area is controlled by a black mask. The average of these PV measurements is 2–3 times. The errors are in the range of 0.6–0.8%. Electrolyte: 0.6 M DMPII, 0.05 M I_2 , 0.5 M TBP, and 0.1 M LiI in acetonitrile.

(EDOT) unit in the ancillary ligand of the ruthenium sensitizer. A slightly higher V_{oc} of JK-206 relative to JK-207 can be correlated with a decrease of the dark current. The J_{sc} enhancement

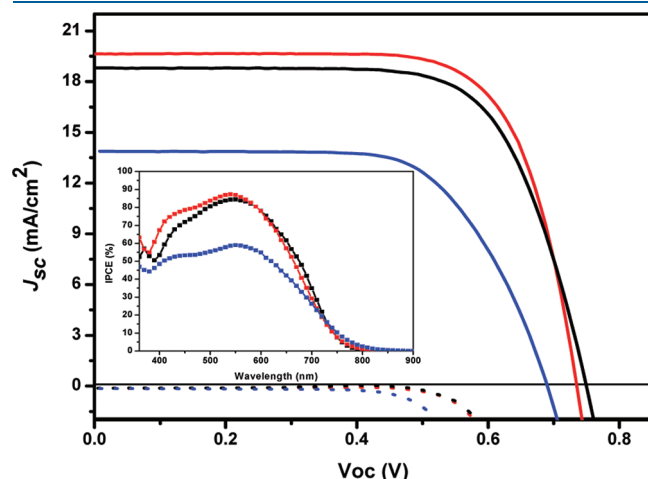


Figure 4. J - V curve and IPCE spectra of JK-206 (red line), JK-207 (blue line), and N719 (black line). The dark current-bias potential relationship is shown as dotted curves.

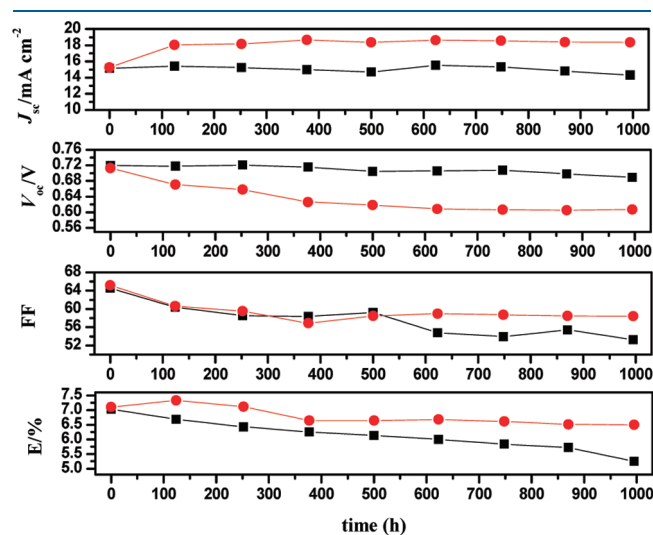
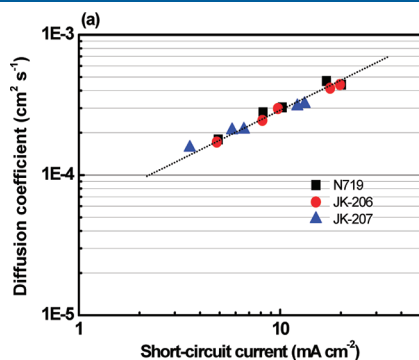


Figure 5. Evolution of solar cell parameters with N719 (black line) and JK-206 (red line) during visible-light soaking (AM 1.5G, 100 mW cm^{-2}) at 60°C . A 420 nm cutoff filter was put on the cell surface during illumination.



of JK-206 compared to JK-207 can be related to the dense packing of the JK-206 monolayer on the TiO_2 electrode. To see the effect of packing in both sensitizers, we measured the amount of dyes adsorbed on the TiO_2 film by desorbing the dyes from the TiO_2 surface with KOH. The amounts of three dyes adsorbed on the TiO_2 film were measured to be 3.84×10^{-7} , 3.04×10^{-7} , and $3.76 \times 10^{-7} \text{ mmol cm}^{-2}$ for JK-206, JK-207, and N719, respectively. The low adsorption of JK-207 can be due to the presence of two bulky EDOT units, the low solubility, and the hydrophilic nature of EDOT. Therefore, the electron recombination occurred more significantly in the photoelectrodes by the ineffective packing of large dyes.

Because long-term stability is a vital element for sustained cell operation, we replaced the liquid electrolyte with a quasi-solid-state one consisting of 0.5 M *N*-methylbenzimidazole (NMBI), 5 wt % PVDF-HFP, 0.6 M DMPII, and 0.1 M I_2 in MPN. The JK-206 sensitized cell yielded a remarkably high conversion efficiency of 7.14% (see Figure 5). After 1000 h of light soaking at 60°C , the initial efficiency of 7.14% in JK-206 decreased to 6.51%. On the other hand, the efficiency of N719 decreased from 7.03% to 5.25% under the same conditions. After 1000 h of light soaking, V_{oc} of JK-206 decreased by 110 mV, but the loss was compensated for by an increase in J_{sc} from 15.27 to 18.35 mA cm^{-2} . The long-term stability of the device is unprecedented because a few ruthenium dyes passed such a severe light-soaking stress by a DSSC with an efficiency of over 6.5%.²⁴ The enhanced long-term stability of JK-206 can be attributed to the intrinsic

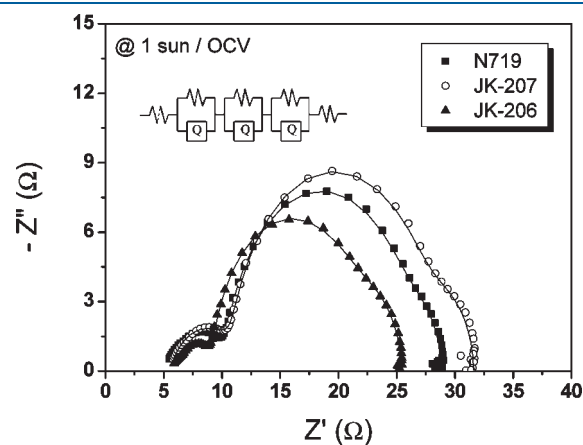


Figure 7. Nyquist plots of EIS spectra measured under illumination of simulated AM 1.5 G (100 mW cm^{-2}) at open-circuit voltage.

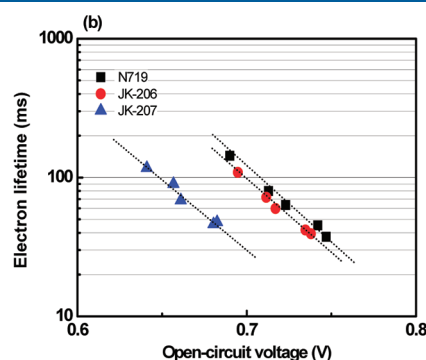


Figure 6. Electron diffusion coefficients (a) and lifetimes (b) of the DSSCs employing JK-206, JK-207, and N719, respectively.

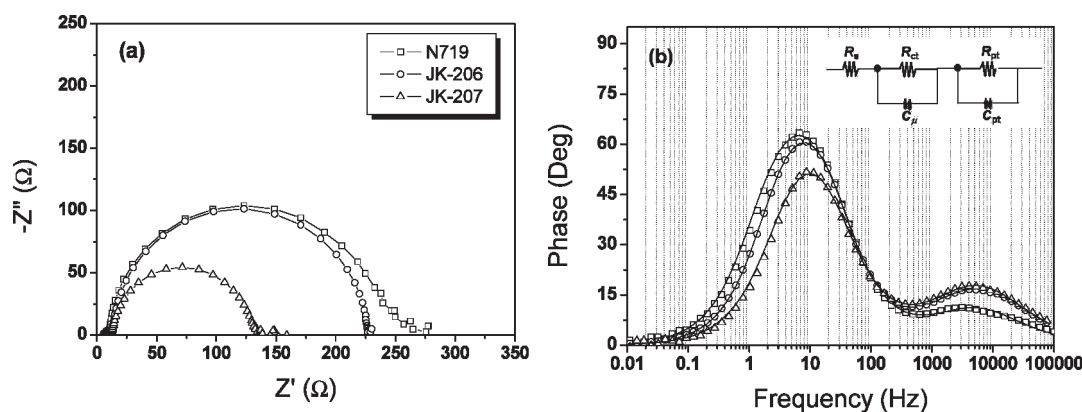


Figure 8. (a) Nyquist plots and (b) Bode phase plots measured in dark conditions at a forward bias of -0.67 V. The inset is the equivalent circuit used to fit the impedance spectra.

stability of a terdentate $\hat{\text{C}}\hat{\text{N}}\hat{\text{N}}$ coordination and the introduction of long alkyl chains to the thienyl ligand.

Figure 6 shows the electron diffusion coefficients (D_e) and lifetimes (τ_e) of the DSSCs employing different dyes JK-206, JK-207, and N719 displayed as a function of J_{sc} and V_{oc} , respectively. No significant differences among the D_e values were seen at identical short-circuit current conditions, showing a trend similar to those of coumarin dyes.²⁵ This result demonstrates that the D_e values are hardly affected by structural changes in the dye molecules. On the other hand, the τ_e values show a significant gap among the dyes, resulting in the increasing order of N719 > JK-206 > JK-207. The different τ_e values might be caused by the different molecular structures of the dyes. The low value of τ_e in JK-207 compared to those of JK-206 and N719 may be due to the defects of the JK-207 monolayer on the TiO_2 electrodes. The results of the electron lifetime are well consistent with those of V_{oc} .

Electrochemical impedance spectroscopy (EIS) was employed to study the electron recombination and electrolyte reduction process in DSSCs based on three dyes. Figure 7 shows the alternating-current impedance spectra of the DSSCs measured under illumination. A smaller radius of the semicircle in this intermediate-frequency regime implies a higher rate of electron transport at the TiO_2 /dye/electrolyte interface. Upon illumination under open-circuit voltage conditions (100 mW cm^{-2}), the response of the intermediate semicircle is attributable to the deposited dye on the TiO_2 /electrolyte. A capacitance (1.1 mF cm^{-2}) of JK-206 derived from $(Y_0 R)(1/n)/R$, where $Y_0 [\text{se}\hat{\text{c}}\hat{\text{n}} \text{ cm}^{-2}]$ is the symbol for the constant phase element, n is the frequency power, and R is the charge-transport resistance, is higher than those of JK-207 (0.49 mF cm^{-2}) and N719 (0.82 mF cm^{-2}), and the resistance of JK-206 (11.98Ω) is low compared with those of JK-207 (16.52Ω) and N719 (15.26Ω). As a result, the photocurrent of JK-206 (19.63 mA cm^{-2}), JK-207 (13.68 mA cm^{-2}), and N719 (18.79 mA cm^{-2}) is in good agreement with the trends observed in the above data.

Figure 8 shows the typical EIS Nyquist and Bode phase plots measured in dark conditions at a forward bias of -0.67 V. The equivalent circuit inset in Figure 8b was used to fit the experimental data of all of the samples. R_s is the series resistance accounting for the transport resistance of the TCO and the electrolyte. C_μ and R_{ct} are the chemical capacitance and the charge recombination resistance at the TiO_2 /electrolyte interface, respectively. C_{pt} and R_{pt} are the interface capacitance and charge-transport resistance at the platinum/electrolyte interface, respectively.

The larger semicircle at the middle-frequency range represents the interfacial charge recombination resistance (R_{ct}) at the dyed TiO_2 /electrolyte interface. The fitted R_{ct} increased in the order of JK-207 (119Ω) < JK-206 (214Ω) < N719 (229Ω), which is consistent with the V_{oc} values measured in the devices. The smaller R_{ct} value means that electron recombination from TiO_2 to electron acceptors in an electrolyte is occurring more easily and thus results in lower V_{oc} . By fitting the EIS curves, another important parameter for DSSCs, the electron lifetime (τ), could be extracted from the C_μ and R_{ct} using $\tau = C_\mu R_{ct}$.^{26,27} Generally, a negative shift of the conduction band edge of TiO_2 leads to improvement of V_{oc} of DSSCs. C_μ increased in the order of N719 ($527 \mu\text{F}$) > JK-207 ($456 \mu\text{F}$) > JK-206 ($410 \mu\text{F}$), and the electron lifetime (τ) increased in the order of N719 (120 ms) > JK-206 (88 ms) > JK-207 (54 ms). Longer electron lifetime contributed to a higher V_{oc} . These results mean that it is the charge recombination resistance, rather than the position of the conduction band edge, that governs V_{oc} . These results were in accordance with the trends of the V_{oc} and τ values.

In conclusion, a new class of cyclometalated ruthenium sensitizers JK-206 and JK-207 was meticulously designed and synthesized. A solar-to-electricity conversion efficiency of 10.39% in JK-206 is better than η of 9.80% for the N719 sensitized cell. The efficiency is the highest one reported for DSSCs based on the cyclometalated ruthenium sensitizer. In addition, the JK-206 sensitized solar cell with a polymer gel electrolyte yielded an overall conversion efficiency of 7.14%. Moreover, the JK-206 device showed excellent stability under light soaking at 60°C for 1000 h. The high efficiency and excellent stability may be attributed to the intrinsic stability of the cyclometalated ruthenium complex with the $\hat{\text{C}}\hat{\text{N}}\hat{\text{N}}$ ligand and the broad and red-shifted absorption property of the cyclometalated complex. We believe that the development of highly efficient DSSC devices with stability is possible through a variety of cyclometalated complexes, and work on these is now in progress.

■ ASSOCIATED CONTENT

S Supporting Information. ^1H and ^{13}C NMR spectra of JK-206 and JK-207, calculated absorption spectra of JK-206, cyclic voltammogram of JK-206, and XYZ coordinates. This material is available free of charge via the Internet at <http://pubs.acs.org>.

AUTHOR INFORMATION

Corresponding Author

*E-mail: jko@korea.ac.kr. Fax: 82 41 867 5396. Tel: 82 41 860 1337.

ACKNOWLEDGMENT

This work was supported by the WCU (the Ministry of Education and Science) program (Grant R31-2008-000-10035-0), the ERC [the Korean government (MEST)] program (Grant R11-2009-088-02001-0), and the New & Renewable Energy of the Korea Institute of Energy Technology Evaluation and Planning (KETEP) grant funded by the Korea government Ministry of Knowledge Economy (Grant 2010T100100674), and computations were performed using a supercomputer at the Korea Institute of Science and Technology Information (Grant KSC-2011-C1-11).

REFERENCES

- (1) (a) O'Ragen, B.; Grätzle, M. *Nature* **1991**, 363, 737. (b) Grätzle, M. *Nature* **2001**, 414, 338.
- (2) (a) Chen, C.-Y.; Chen, J.-G.; Wu, S.-J.; Li, J.-Y.; Wu, C.-G.; Ho, K.-C. *Angew. Chem., Int. Ed.* **2008**, 47, 7342. (b) Wang, P.; Klein, C.; Humphry-Baker, R.; Zakeeruddin, S. M.; Grätzel, M. *J. Am. Chem. Soc.* **2005**, 127, 808. (c) Jiang, K.-J.; Masaki, N.; Xia, J.; Noda, S.; Yanagida, S. *Chem. Commun.* **2006**, 2460.
- (3) (a) Choi, H.; Kim, S.; Kang, S. O.; Ko, J.; Kang, M.-S.; Clifford, J. N.; Forneli, A.; Palomares, E.; Nazeeruddin, M. K.; Grätzel, M. *Angew. Chem., Int. Ed.* **2008**, 47, 8259. (b) Clifford, J. N.; Palomares, E.; Nazeeruddin, M. K.; Thampi, R.; Grätzel, M.; Durrant, J. R. *J. Am. Chem. Soc.* **2004**, 126, 5670.
- (4) (a) Wang, P.; Zakeeruddin, S. M.; Humphry-Baker, R.; Grätzel, M. *Chem. Mater.* **2004**, 16, 2694. (b) Wang, P.; Zakeeruddin, S. M.; Humphry-Baker, R.; Mser, J. E.; Grätzel, M. *Adv. Mater.* **2003**, 15, 2101.
- (5) Chiba, Y.; Islam, A.; Wantanabe, Y.; Komiya, R.; Koide, N.; Han, L. *Jpn. J. Appl. Phys., Part 2* **2006**, 45, L638.
- (6) Anderson, P. A.; Strouse, G. F.; Treadway, T. A.; Keene, F. R.; Meyer, T. J. *Inorg. Chem.* **1994**, 33, 3863.
- (7) (a) Jang, S.-R.; Lee, C.; Choi, H.; Ko, J.; Lee, J.; Vittal, R.; Kim, K.-J. *Chem. Mater.* **2006**, 18, 5604. (b) Kim, C.; Choi, H.; Kim, S.; Baik, C.; Song, K.; Kang, M.-S.; Kang, S. O.; Ko, J. *J. Org. Chem.* **2008**, 73, 7072. (c) Lee, C.; Yum, J.-H.; Choi, H.; Kang, S. O.; Ko, J.; Humphry-Baker, R.; Grätzel, M.; Nazeeruddin, M. K. *Inorg. Chem.* **2008**, 47, 2267. (d) Kim, J.-J.; Lim, K.; Choi, H.; Fan, S.; Kang, M.-S.; Gao, G.; Kang, H. S.; Ko, J. *Inorg. Chem.* **2010**, 49, 8351.
- (8) (a) Chen, C.-Y.; Wu, S.-J.; Li, J.-Y.; Wu, C.-G.; Chen, J.-G.; Ho, K.-C. *Adv. Mater.* **2007**, 19, 3888. (b) Abbotto, A.; Barolo, C.; Bellotto, L.; De Angelis, F.; Grätzel, M.; Manfredi, N.; Marini, C.; Fantacci, S.; Yum, J.-H.; Nazeeruddin, M. K. *Chem. Commun.* **2008**, 5318. (c) Kim, J.-J.; Choi, H.; Kim, C.; Kang, M.-S.; Kang, H. S.; Ko, J. *Chem. Mater.* **2009**, 21, 5719.
- (9) (a) Wang, P.; Zakeeruddin, S. M.; Moser, J.-E.; Humphry-Baker, R.; Comte, P.; Aranyos, V.; Hagfeldt, A.; Nazeeruddin, M. K.; Grätzel, M. *Adv. Mater.* **2004**, 16, 1806. (b) Kuang, D.; Klein, C.; Ito, S.; Moser, J.-E.; Humphry-Baker, R.; Evans, N.; Durrant, J.; Grätzel, C.; Zakeeruddin, S. M.; Grätzel, M. *Adv. Mater.* **2007**, 19, 1133.
- (10) (a) Wadman, S. H.; Lutz, M.; Tooke, D. M.; Spek, A. L.; Hartl, F.; Havenith, R. W. A.; van Klink, G. P. N.; van Koten, G. *Inorg. Chem.* **2009**, 48, 1887. (b) Bomben, P. G.; Robson, K. C. D.; Sedach, P. A.; Berlinguette, C. P. *Inorg. Chem.* **2009**, 48, 9631. (c) Bomben, P. G.; Koivisto, B. D.; Berlinguette, C. P. *Inorg. Chem.* **2010**, 49, 4960.
- (11) Bessho, T.; Yoneda, E.; Yum, J.-H.; Guglielmi, M.; Tavernelli, I.; Imai, H.; Rothlisberger, U.; Nazeeruddin, M. K.; Grätzel, M. *J. Am. Chem. Soc.* **2009**, 131, 5930.
- (12) (a) Kisserwan, H.; Ghaddar, T. H. *Dalton Trans.* **2011**, 40, 3877. (b) Wadman, S. H.; Kroon, J. M.; Bakker, K.; Lutz, M.; Spek, A. L.; van Klink, G. P. M.; van Koten, G. *Chem. Commun.* **2007**, 1907.
- (13) (a) Wu, K.-L.; Hsu, H.-C.; Chen, K.; Chi, Y.; Chung, M.-W.; Chou, P.-T. *Chem. Commun.* **2010**, 46, 5124. (b) Chou, C.-C.; Wu, K.-L.; Chi, Y.; Hu, W.-P.; Yu, S. J.; Lee, G.-H.; Lin, C.-L.; Chou, P.-T. *Angew. Chem., Int. Ed.* **2011**, 50, 2054. (c) Chen, K.-S.; Liu, W.-H.; Wang, Y.-H.; Lai, C.-H.; Chou, P.-T.; Lee, G.-H.; Chen, K.; Chen, H.-Y.; Chi, Y.; Tung, F.-C. *Adv. Funct. Mater.* **2007**, 17, 2964.
- (14) Islam, A.; Chowdhury, F. A.; Chiba, Y.; Komiya, R.; Fuke, N.; Ikeda, N.; Nozaki, K.; Han, L. *Chem. Mater.* **2006**, 18, 5178.
- (15) Wiederholt, K.; McLaughlin, L. W. *Nucleic Acids Res.* **1999**, 27, 2487.
- (16) Gao, F.; Wang, Y.; Shi, D.; Zhang, J.; Wang, M.; Jing, X.; Humphry-Baker, R.; Wang, P.; Zakeeruddin, S. M.; Grätzel, M. *J. Am. Chem. Soc.* **2008**, 130, 10720.
- (17) Shi, D.; Pootrakulchote, N.; Li, R.; Gui, J.; Wang, Y.; Zakeeruddin, S. M.; Grätzel, M.; Wang, P. *J. Phys. Chem. C* **2008**, 112, 17046.
- (18) (a) Stoyanov, S. R.; Villegas, J. M.; Rillema, D. P. *Inorg. Chem.* **2003**, 42, 7852. (b) Jin, Z.; Masuda, H.; Yamanaka, N.; Minami, M.; Nakamura, T.; Nishikitani, Y. *J. Phys. Chem. C* **2009**, 113, 2618.
- (19) Frisch, M. J.; Trucks, G. W.; Schlegel, H. B.; Scuseria, G. E.; Robb, M. A.; Cheeseman, J. R.; Montgomery, J. A., Jr.; Vreven, T.; Kudin, K. N.; Burant, J. C.; Millam, J. M.; Iyengar, S. S.; Tomasi, J.; Barone, V.; Mennucci, B.; Cossi, M.; Scalmani, G.; Rega, N.; Petersson, G. A.; Nakatsuji, H.; Hada, M.; Ehara, M.; Toyota, K.; Fukuda, R.; Hasegawa, J.; Ishida, M.; Nakajima, T.; Honda, Y.; Kitao, O.; Nakai, H.; Klene, M.; Li, X.; Knox, J. E.; Hratchian, H. P.; Cross, J. B.; Adamo, C.; Jaramillo, J.; Gomperts, R.; Stratmann, R. E.; Yazyev, O.; Austin, A. J.; Cammi, R.; Pomelli, C.; Ochterski, J. W.; Ayala, P. Y.; Morokuma, K.; Voth, G. A.; Salvador, P.; Dannenberg, J. J.; Zakrzewski, V. G.; Dapprich, S.; Daniels, A. D.; Strain, M. C.; Farkas, O.; Malick, D. K.; Rabuck, A. D.; Raghavachari, K.; Foresman, J. B.; Ortiz, J. V.; Cui, Q.; Baboul, A. G.; Clifford, S.; Cioslowski, J.; Stefanov, B. B.; Liu, G.; Liashenko, A.; Piskorz, P.; Komaromi, I.; Martin, R. L.; Fox, D. J.; Keith, T.; Al-Laham, M. A.; Peng, C. Y.; Nanayakkara, A.; Challacombe, M.; Gill, P. M. W.; Johnson, B.; Chen, W.; Wong, M. W.; Gonzalez, C.; Pople, J. A. *Gaussian03*, revision B.05; Gaussian, Inc.: Pittsburgh, PA, 2003.
- (20) (a) Nakade, S.; Kanzaki, T.; Wada, Y.; Yanagida, S. *Langmuir* **2005**, 21, 10803. (b) Kang, M.-S.; Ahn, K.-S.; Lee, J.-W.; Kang, Y. S. *J. Photochem. Photobiol. A: Chem.* **2008**, 195, 198. (c) Ahn, K.-S.; Kang, M.-S.; Lee, J.-K.; Shin, B.-C.; Lee, J.-W. *Appl. Phys. Lett.* **2006**, 89, 013103.
- (21) (a) Hoffmann, K. J.; Bakken, E.; Samuelsen, E. J.; Carlsen, P. H. *J. Synth. Met.* **2000**, 113, 39. (b) Huang, C.-H.; McClenaghan, N. D.; Kuhn, A.; Hofstraat, J. W.; Bassan, D. M. *Org. Lett.* **2005**, 7, 3409. (c) Turbiez, M.; Frère, P.; Allain, M.; Videlot, C.; Ackermann, J.; Roncali, J. *Chem.—Eur. J.* **2005**, 11, 3742.
- (22) Nazeeruddin, M. K.; Kay, A.; Rodicio, I.; Humphry-Baker, R.; Muller, E.; Liska, P.; Vlachopoulos, N.; Grätzel, M. *J. Am. Chem. Soc.* **1993**, 115, 6382.
- (23) (a) Bond, A. M.; Deacon, G. B.; Howitt, J.; MacFarlane, D. R.; Spiccia, L.; Wolfbauer, G. *J. Electrochem. Soc.* **1999**, 146, 648. (b) Wang, P.; Zakeeruddin, S. M.; Moser, J.-E.; Grätzel, M. *J. Phys. Chem. B* **2003**, 107, 13280.
- (24) (a) Wang, Q.; Moser, J.-E.; Grätzel, M. *J. Phys. Chem. B* **2005**, 109, 14945. (b) Wang, P.; Zakeeruddin, S. M.; Moser, J. E.; Nazeeruddin, M. K.; Sekiguchi, T.; Grätzel, M. *Nat. Mater.* **2003**, 2, 402.
- (25) Hara, K.; Miyamoto, K.; Abe, Y.; Yanagida, M. *J. Phys. Chem. B* **2005**, 109, 23776.
- (26) Wang, Q.; Ito, S.; Grätzel, M.; Fabregat-Santiago, F.; Mora-Seró, I.; Bisquert, J.; Bessho, T.; Imai, H. *J. Phys. Chem. B* **2006**, 110, 25210.
- (27) Bisquert, J.; Fabregat-Santiago, F.; Mora-Seró, I.; Garcia-Belmonte, G.; Giménez, S. *J. Phys. Chem. C* **2009**, 113, 17278.